Cerebral Cortex December 2012;22:2761–2768
doi:10.1093/cercor/bhr355
Advance Access publication December 15, 2011

White Matter Aberrations in Prepubertal Estrogen-Naive Girls with Monosomic Turner Syndrome

Bun Yamagata[1,2], Naama Barnea-Goraly[1], Matthew J. Marzelli[1], Yaena Park[1], David S. Hong[1], Masaru Mimura[2] and Allan L. Reiss[1,3]

[1]Center for Interdisciplinary Brain Sciences Research, Department of Psychiatry and Behavioral Sciences, Stanford University School of Medicine, Stanford, CA 94305, USA, [2]Department of Neuropsychiatry, Showa University School of Medicine, Tokyo 157-8577, Japan and [3]Department of Radiology, Stanford University School of Medicine, Stanford, CA 94305, USA

Yamagata and Barnea-Goraly have contributed equally to this work

Address correspondence to Allan L. Reiss, Center for Interdisciplinary Brain Sciences Research, Department of Psychiatry and Behavioral Sciences, Stanford University School of Medicine, Stanford, CA 94305, USA. Email: areiss1@stanford.edu.

Turner syndrome (TS) offers a unique opportunity to investigate associations among genes, the brain, and cognitive phenotypes. In this study, we used 3 complementary analyses of diffusion tensor imaging (DTI) data (whole brain, region of interest, and fiber tractography) and a whole brain volumetric imaging technique to investigate white matter (WM) structure in prepubertal, nonmosaic, estrogen-naive girls with TS compared with age and sex matched typically developing controls. The TS group demonstrated significant WM aberrations in brain regions implicated in visuospatial abilities, face processing, and sensorimotor and social abilities compared with controls. Extensive spatial overlap between regions of aberrant WM structure (from DTI) and regions of aberrant WM volume were observed in TS. Our findings indicate that complete absence of an X chromosome in young females (prior to receiving exogenous estrogen) is associated with WM aberrations in specific regions implicated in characteristic cognitive features of TS.

Keywords: diffusion tensor imaging (DTI), MRI, neuroimaging, turner syndrome, voxel-based morphometry (VBM)

Introduction

Turner syndrome (TS) is a neurogenetic disorder characterized by partial or complete absence of an X chromosome, affecting approximately 1 in 2000 live female births (Gravholt 2005). The TS phenotype is characterized by short stature and also by gonadal dysgenesis, which results in estrogen deficiency, incomplete pubertal development, and infertility. In addition, girls with TS manifest a cognitive profile of relative strengths in verbal domains and relative weaknesses in visuospatial, executive, memory (Kesler 2007), motor (Nijhuis-van der Sanden et al. 2003), and social functions (McCauley et al. 2001). These phenotypes may be affected by nonmosaic/mosaic karyotypes of the sex chromosome, the presence of partial X and Y chromosome fragments, and the presence of X-linked imprinting (Skuse et al. 1997).

Structural magnetic resonance imaging (sMRI) studies have demonstrated that adolescents and adults with TS have reduced gray matter volume (GMV) in the parieto-occipital lobe (Cutter et al. 2006) and enlarged GMV in the amygdala (Kesler, Garrett, et al. 2004) compared with controls. A recent brain sMRI study also identified increased cortical thickness and decreased surface area in TS compared with controls in parietal and occipital lobes (Raznahan et al. 2010). Functional MRI (fMRI) studies of TS have indicated that deficits in visuospatial and arithmetic processing in TS are associated with functional impairment in fronto-parietal systems (Kesler, Haberecht, et al. 2004), whereas deficits in executive function and storage/retrieval operations are associated with decreased activation in the inferior parietal lobe, dorsolateral prefrontal cortex, and the caudate (Haberecht et al. 2001). To date, 2 studies (Molko et al. 2004; Holzapfel et al. 2006) have specifically focused on aberrant white matter (WM) structure in TS using diffusion tensor imaging (DTI), which is a non-invasive MRI technique that characterizes water diffusion in the brain. These studies suggested that WM aberrations in the superior temporal sulcus and fronto-parietal pathways could be related to social and visuospatial deficits in TS, respectively. However, these studies are limited by several factors. For instance, they include heterogeneous samples with mosaic and nonmosaic genotypes and do not examine the relationship between cognitive data and WM structure. In addition, previous imaging studies of WM in TS have not directly examined the influence of between-group differences in overall cognitive ability or the effects of estrogen therapy on brain development. Accordingly, little information is available about WM aberrations in nonmosaic, pre-estrogen girls with TS.

In this study, we used complementary image analysis techniques to investigate WM structure and its correlations with cognitive functions in nonmosaic, estrogen-naive girls with TS. The results of this investigation permit an improved understanding of the effects of complete absence of an X chromosome on early WM development and cognition in young girls, while removing the confounding influence of exogenous estrogen. The present study includes 3 methods for analyzing diffusion-weighted brain imaging data. First, we performed a WM voxel-wise analysis using Tract-based Spatial Statistics (TBSS) implemented in FSL (www.fmrib.ox.ac.uk/fsl/tbss) (Smith et al. 2006). Second, we used 2 post hoc confirmatory analyses to provide complementary information to TBSS; an atlas-based region of interest (ROI) analysis implemented in DiffeoMap (www.mristudio.org) (Faria et al. 2010) and a fiber-tracking analysis using DtiStudio (www.mristudio.org) (Jiang et al. 2006). Finally, we performed a voxel-wise analysis of WM volume (WMV) using voxel-based morphometry (VBM) as implemented in SPM8 (www.fil.ion.ucl.ac.uk/spm). The use of these multiple complementary methods serves to provide more reliable and complete information about WM structure by minimizing inherent disadvantages associated with a single imaging modality or image processing approach (i.e., partial volume effects, smoothing, and registration error).

Based on the phenotype of TS and previous neuroimaging findings, we hypothesized that girls with TS would have aberrant WM structure in regions associated with executive, visual,

memory, sensorimotor, and social functions. Furthermore, we hypothesized that these WM aberrations would be associated with severity of cognitive impairment in TS.

Materials and Methods

Participants

This study was approved by the Institutional Review Board at Stanford University. Participants included 26 subjects with TS and 20 age-matched typically developing controls ranging 3–12 years in age. None of the participants had evidence of current or past major neurological and psychiatric problems. Girls with TS were recruited through the national Turner Syndrome Society of the United States, advertisements in local parent organizations, and the Center for Interdisciplinary Brain Sciences Research website (http://cibsr.stanford.edu). Only TS subjects with a nonmosaic 45X karyotype, confirmed from a standard karyotype assessment, were included. Twenty participants with TS were receiving growth hormone (GH) at the time of the study; however, data regarding the duration and dosage of GH therapy were unavailable. Controls were recruited through local media and parent networks. We obtained written informed consent from all participants and their legal guardian. If the subject was under 8 years old, consent was obtained only from the legal guardian.

Cognitive Assessment

Participants between the ages of 3 and 5 years were administered the Wechsler Preschool and Primary Scale of Intelligence-Third Edition (WPPSI-III) (Wechsler 2002). Children aged 6–12 years were administered the Wechsler Intelligence Scale for Children-Fourth Edition (WISC-IV) (Wechsler 2003). Participants demonstrating full-scale intelligence quotient (FSIQ) below 70 were excluded from further analyses to avoid confounding effects. Accordingly, 3 girls with TS were eliminated from further analysis. We further evaluated executive, visual, memory, sensorimotor, and social functions using cognitive measures (Table 1). During the course of subject recruitment, the Developmental Neuropsychological Assessment-II (NEPSY-II) (Korkman and Kirk 2007) was released, which introduced a new Social Perception domain, including Affect Recognition and Theory of Mind subscales. Therefore, while all subjects were assessed with the Developmental Neuropsychological Assessment (NEPSY) (Korkman and Kirk 1998); a subset received the NEPSY-II as well. WISC-IV Working Memory Index was administered only to participants aged 6–12 years. Potential between-group differences in age, major IQ, and cognitive measure scores were initially evaluated using independent two-tailed Student's *t*-tests. The Social Responsiveness Scale (Constantino et al. 2003) is not specifically age-normed; thus, age was included as a covariate in analyses using this instrument. Since the WISC Perceptual Reasoning Index/WPPSI PIQ and NEPSY-II Social Perception domain consist of several subtests, we performed a multivariate analysis of variance using these subscale scores as dependent variables.

Image Acquisition

All subjects were trained in the MRI scanning procedure using a mock scanner. MR images were acquired using a 3T whole-body GE-Signa HDxt scanner (GE Medical Systems, Milwaukee, WI) with a quadrature head coil. A diffusion-weighted sequence was based on a single-shot, spin-echo, echo-planar imaging sequence with diffusion sensitizing gradients applied on either side of the 180° refocusing pulse (Basser et al. 1994). Imaging parameters for the diffusion-weighted sequence were as follows: field of view (FOV), 24 cm; matrix size, 128 × 128; time repetition (TR)/time echo (TE), 5910/70.3 ms; 44 axial-oblique slices; slice thickness, 3.2 mm/no skip. Diffusion gradient duration was $\delta = 32$ ms and diffusion weighting was $b = 850$ s/mm^2 and $b = 0$ as reference images. Diffusion was measured along 23 noncollinear directions. This pattern was repeated 6 times. For VBM, high-resolution T_1-anatomical scans were obtained using a spoiled gradient recalled echo pulse sequence (124 coronal slices; TR/TE, 6.4/2 ms; inversion time, 300 ms; flip angle, 15°; NEX, 3; FOV, 22 cm; matrix, 256 × 256; thickness, 1.5 mm; acquisition time, 15 min 45 s).

Image Processing and Statistical Analysis

Diffusion-Weighted Scans Preprocessing

Diffusion-weighted images (DWIs) were corrected for eddy current distortions and head motion using a3n affine transformation of

Table 1

Demographics, intelligence quotient, and cognitive measures

			DTI				VBM			
			TS	CON	*P*		TS	CON	*P*	
Demographic data and intelligence quotient										
n			26	20			16	13		
Age			8.51 ± 2.56	8.27 ± 2.77	0.769		8.84 ± 2.49	8.37 ± 2.87	0.644	
FSIQ			92.31 ± 14.75	116.0 ± 10.49	<0.001		94.06 ± 9.00	114.15 ± 11.89	<0.001	
VIQ			103.08 ± 14.49	114.75 ± 13.58	<0.01		106.31 ± 10.56	113.92 ± 13.37	0.098	
PIQ			90.38 ± 15.72	115.6 ± 13.62	<0.001		92.69 ± 9.03	112.46 ± 13.19	<0.001	
Cognitive and behavioral measures										
Cognitive domain	Test	Subtest	TS	CON	*F*	*P*	TS	CON	*F*	*P*
Executive	NEPSY	Attention/executive total	89.96 ± 15.15	105.17 ± 12.76	6.41	0.011	92.88 ± 14.09	109.25 ± 11.85	7.59	0.003
Visual	NEPSY	Visuospatial total	82.35 ± 12.67	103.72 ± 16.05	19.46	<0.0001	80.31 ± 11.83	105.58 ± 13.42	22.95	<0.0001
	WISC/WPPSI	Block design	8.54 ± 3.06	12.05 ± 2.83	6.33	<0.001	9.13 ± 2.32	11.42 ± 3.28	2.48	0.042
		Picture concept	8.71 ± 4.03	12.53 ± 2.32	5.79	0.001	8.73 ± 3.75	12.00 ± 1.90	5.08	0.011
		Matrix reasoning	8.67 ± 2.99	13.05 ± 2.99	12.36	<0.0001	9.07 ± 2.49	12.58 ± 3.08	6.99	0.003
Memory	NEPSY	Memory and learning total	93.88 ± 14.50	112.22 ± 21.68	5.45	0.002	91.13 ± 12.31	113.0 ± 17.3	10.63	0.001
	WISC	WMI total[a]	83.55 ± 10.82	106.50 ± 10.58	24.67	<0.0001	84.38 ± 12.75	105.67 ± 11.18	10.62	0.001
Sensorimotor	NEPSY	Sensorimotor total	85.04 ± 13.21	109.83 ± 11.40	30.71	<0.0001	86.81 ± 14.56	109.25 ± 13.17	14.31	<0.001
	WRAVMA	Pegboard	75.38 ± 17.99	100.84 ± 13.30	18.27	<0.0001	73.69 ± 17.06	105.50 ± 12.93	20.23	<0.0001
Social	NEPSY	Memory for faces	9.25 ± 2.75	13.13 ± 3.02	13.91	<0.0001	8.94 ± 2.46	13.10 ± 3.34	12.44	0.001
	NEPSY-II	Theory of mind[b]	9.50 ± 2.35	10.50 ± 2.42	0.47	0.485	8.67 ± 2.88	10.50 ± 1.73	0.46	0.602
		Affect recognition[b]	7.83 ± 2.78	10.50 ± 1.64	3.65	0.071	9.33 ± 2.08	10.50 ± 3.10	0.30	0.078
	SRS	Total	61.30 ± 14.93	49.93 ± 13.99	4.69	0.026	63.33 ± 13.65	47.60 ± 13.24	8.64	0.01
	RCMAS-2	Total	45.65 ± 9.69	40.00 ± 9.92	1.28	0.124	45.80 ± 8.32	38.00 ± 7.31	4.51	0.039

Note: CON, controls; VIQ, Verbal Intelligence Quotient; PIQ, Performance Intelligence Quotient; NEPSY, Developmental Neuropsychological Assessment; WISC WMI, WISC Working Memory Index; WRAVMA, Wide Range Assessment of Visual Motor Abilities; NEPSY-II, Developmental Neuropsychological Assessment-Second Edition; SRS, Social Responsiveness Scale; RCMAS-2, Revised Children's Manifest Anxiety Scale-Second Edition.

[a]TS ($n = 20$), CON ($n = 14$) in DTI; TS ($n = 13$), CON ($n = 9$) in VBM.

[b]TS ($n = 16$), CON ($n = 16$) in DTI; TS ($n = 10$), CON ($n = 10$) in VBM.

Automated Image Registration (Woods et al. 1998). All individual images were visually inspected to eliminate slices with motion artifacts. We excluded 6 subjects from further analysis because of significant artifacts. The remaining images were averaged and the pixel intensities of the multiple DWIs were then fitted to obtain the 6 elements of the symmetric diffusion tensor. Scalars such as fractional anisotropy (FA), axial diffusivity (AD), and radial diffusivity (RD) were calculated using DTIStudio (https://www.mristudio.org/). FA is a measure that reflects the degree of diffusion anisotropy within a voxel. Anisotropy within a given WM voxel is determined by fiber diameter and density, degree of myelination, extracellular diffusion, interaxonal spacing, and intravoxel fiber-tract coherence. AD is the diffusivity of water molecules along the axis of the fiber (vector with the largest eigenvalue, $\lambda 1$) and RD is the mean of the diffusivities perpendicular to the vector with the largest eigenvalue ($[\lambda 2 + \lambda 3]/2$). AD is thought to reflect fiber coherence, whereas RD is thought to represent fiber integrity and myelination.

TBSS

First, FA images from each subject were aligned into a common space using nonlinear and linear registrations. Subsequently, FA images were averaged to produce a group mean FA image. A skeletonization algorithm was applied to the group mean FA image to define a group template of the lines of maximum FA, thought to correspond to centers of WM tracts. FA values for each subject were then projected onto the group template skeleton. The FA skeleton was thresholded to FA $\geqslant$ 0.25. The original registration parameters of the FA were then applied to the AD and RD images. FA, AD, and RD data projected onto the skeleton were fed into voxel-wise cross-subject statistics ($P < 0.05$) using "randomize" (v. 2.1 in FSL4.1), a permutation program used for inference (thresholding) on statistic maps when the null distribution is not known (Nichols and Holmes 2002). All analyses were corrected for multiple comparisons (family-wise error [FWE]) and used threshold-free cluster enhancement (TFCE) (Smith and Nichols 2009) with default parameters. Age and verbal IQ (VIQ) were used as covariates. VIQ was used as the covariate for further analyses as performance IQ (PIQ) scores are disproportionally biased by visual perceptual and visual spatial deficits present in girls with TS (Kesler, Haberecht, et al. 2004).

Atlas-Based Analysis

We used an exploratory atlas–based approach as a confirmatory analysis of TBSS findings. In this approach, brain regions showing between-group FA differences in TBSS were used to select predefined WM atlas ROI's. A univariate analysis of covariance (ANCOVA) was used to compare between-group differences of mean FA, AD, and RD values in each ROI. Age and VIQ were included as covariates.

A two-step image transformation was used to warp an atlas to individual native space. A skull stripped "JHU_MNI_single-subject" atlas (Oishi et al. 2009) was used for the linear and nonlinear normalization of FA images. Dual-contrast Large Deformation Diffeomorphic Metric Mapping (Ceritoglu et al. 2009) was used for nonlinear normalization (single α/γ ratio was 0.005). The inverse transformation matrices were then used to transfer the presegmented WM atlas (Oishi et al. 2009) to each subjects native space, thus enabling the automated segmentation of the data into 130 WM regions using an FA threshold of 0.25. The transformation matrix from the FA was then applied to the original AD and RD images to obtain segmented values from these images.

Fiber Tracking

Fiber tracking was performed using the fiber assignment by continuous tracking method (Mori et al. 1999). Briefly, tracking was initiated from a seed pixel from which a line was propagated in both retrograde and orthograde directions according to an eigenvector at each pixel. The tracking was terminated when it reached a pixel with an FA value lower than 0.15 or when the turning angle was >40° (Wakana et al. 2004). To reconstruct branching patterns, the tracking was performed at every pixel inside the brain, but only fibers that penetrated ROIs defined from anatomical landmarks were retained. Mean FA, AD, and RD values were collected for each reconstructed fiber bundle. ANCOVA was used to compare the between group difference of FA, AD, and RD values in each hemispheric ROI using age and VIQ as covariates.

VBM

T_1 image data for the subjects that were included in the DTI analyses were visually inspected to eliminate scans with significant head motion artifact in an effort to prevent confounds due to systematic bias. Accordingly, 17 scans were eliminated from further analysis. The remaining scans were manually aligned onto the axis of the anterior and posterior commissures (Talairach and Tournoux 1988). SPM8 was then employed in MATLAB (The Math Works, Natick, MA) to correct for inhomogeneity of the magnetic field and to perform unified segmentation of the GM, WM, and cerebrospinal fluid (Ashburner and Friston 2005). In doing so, adult tissue probability maps were used in conjunction with iterative weighting of Hidden Markov Ransom Fields to encode spatial information based on constraints of neighboring voxels (Zhang et al. 2001). Warped and modulated images were then created in Montreal Neurological Institute space using a custom WM template that was generated based on registration of each subject's image volume using the Diffeomorphic Anatomical Registration Through Lie Algebra toolbox (Ashburner 2007). Finally, all images were spatially smoothed using a 3D 6-mm full-width at half-maximum Gaussian smoothing kernel. Differences in total GMV and WMV between groups were evaluated using a two-sample *t*-test (adjusted for age and VIQ). Between-group morphological differences of regional WMV between TS and control subjects were investigated by applying the general linear model in SPM8. Accordingly, a voxel-wise two-sample *t*-test was performed while covarying for the effects of age, VIQ, and WMV. Statistical inference of significant clusters was then evaluated using the VBM toolbox (Christian Gaser, University of Jena; dbm.neuro.uni-jena.de/vbm/) at a height of $P < 0.01$, spatial extent $P < 0.05$ (FWE corrected), while applying nonstationary cluster extent correction to account for nonuniform smoothness across the data (Hayasaka et al. 2004).

Behavioral Correlations

In the TS group, we investigated the relationship between cognitive measures and mean FA, AD, and RD values (derived from the atlas-based analysis). Multiple regression analysis was performed in regions showing significant mean FA differences by modeling FA, AD, and RD values as dependent variables and by modeling cognitive measures, age, and IQ as predictor variables. Statistical significance was defined as $P < 0.05$, and all analyses were performed using SPSS (Version 18) except for TBSS and VBM analyses.

Results

Demographics and Cognitive Measures

Twenty-six girls with TS and 20 controls were included in DTI analyses. There were no significant differences in age between the groups. Girls with TS had significantly lower FSIQ, VIQ, and PIQ scores compared with controls (Table 1). Girls with TS also showed significantly lower performance compared with controls on all neuropsychological domains with the exception of the NEPSY-II Theory of Mind, Affect Recognition, and Revised Children's Manifest Anxiety Scale-Second Edition (Reynolds and Richmond 1997) total score. After screening for and eliminating anatomical scans that had head motion, a subgroup of 16 girls with TS and 13 controls were included in the VBM analysis (Table 1). This reduction in sample size is due to the long acquisition time of the anatomical scan (15 min), which negatively affected the yield of usable data. In contrast, the DTI acquisition consisted of 6 serial repetitions (2.5 min each); extracting usable data from the first 2 repetitions (totaling 5 min) was considered the threshold for entering the subject into the DTI analysis. Cognitive measures in the VBM subgroup displayed similar characteristics to the DTI subject group (Table 1). When using VIQ as a covariate to account for variations related to individual intelligence, cognitive measures

in both DTI and VBM subgroups revealed similar between-group characteristics to those observed without covarying VIQ.

TBSS

Girls with TS had significant widespread reductions in FA values compared with controls (Fig. 1). These reductions were observed bilaterally in the superior longitudinal fasciculus (SLF; more prominent on the left), inferior longitudinal fasciculus (ILF; more prominent on the left), inferior fronto-occipital fasciculus (IFO), fusiform gyrus WM approaching the amygdala, internal capsule (IC), corticospinal tract (CST), corpus callosum (CC; in the genu, body, and splenium), and tapetum. In addition, FA was also significantly reduced bilaterally in the forceps major, anterior thalamic radiation, posterior thalamic radiation (PTR), sagittal stratum, and posterior corona radiata (PCR). Unilateral FA reductions were identified in the right superior temporal gyrus (STG) WM and in the left forceps minor, frontal corona radiata, and external capsule. There were no significantly increased FA values in TS compared with controls. TS showed significantly greater RD compared with controls in the regions overlapping those that had significant FA group differences. Increased AD in TS compared with controls was seen bilaterally in the SLF, ILF, posterior corona radiata, and external capsule. However, these WM regions did not overlap with those of our FA findings.

Atlas-Based Analysis

A post hoc confirmatory atlas-based analysis was conducted in an openly exploratory manner. We defined 36 ROIs based on TBSS results. ANCOVA indicated that TS had significantly decreased FA values compared with controls in the left SLF ($F_{1,42}$ = 4.84, P = 0.033), left fusiform WM ($F_{1,42}$ = 8.22, P = 0.006), left anterior limb of the internal capsule (ALIC; $F_{1,42}$ = 15.6, P < 0.001), bilateral tapetum (left: $F_{1,42}$ = 7.22, P = 0.01; right: $F_{1,42}$ = 13.57, P = 0.001), bilateral gene of CC (left: $F_{1,42}$ = 8.19, P = 0.007; right: $F_{1,42}$ = 5.58, P = 0.02), right splenium of CC ($F_{1,42}$ = 5.58, P = 0.023), right STG WM ($F_{1,42}$ = 10.78, P = 0.002), and bilateral PTR (left: $F_{1,42}$ = 6.55, P = 0.014; right: $F_{1,42}$ = 10.4, P = 0.002). Relative to controls, TS showed significantly increased AD in the right SLF (P = 0.026), right tapetum (P = 0.03), right STG WM (P = 0.017), left PTR (P = 0.025), and bilateral PCR (left: P = 0.004; right: P < 0.001). Significantly higher RD in TS was observed in the left SLF (P = 0.014), bilateral tapetum (left: P = 0.025; right: P = 0.005), bilateral PTR (left: P = 0.037; right: P < 0.001), and bilateral PCR (P = 0.008; right: P = 0.023).

Fiber Tracking

A post hoc fiber-tracking analysis of the SLF was performed. We chose the SLF for further investigation because it is the only distinct WM fiber bundle that was found to be significantly different using TBSS, VBM, and post hoc atlas-based analysis. In this study, the ROI for the SLF does not include the arcuate fasciculus (Wakana et al. 2004). TS had significantly decreased FA values in the left SLF ($F_{1,42}$ = 4.27, P = 0.045) and increased RD in the bilateral SLF (left: $F_{1,42}$ = 4.93, P = 0.032; right: $F_{1,42}$ = 5.93, P = 0.019) compared with controls. There was no significant group effect for AD values in the bilateral SLF.

VBM

There were no significant differences in total GMV and WMV between TS and controls (adjusted for age and VIQ). Additionally, visual inspection of the location of significant clusters from whole-brain voxel-wise analysis of WM morphology in TS identified reduced WMV (P < 0.05, FWE corrected) unilaterally in the right SLF extending into the pre/postcentral gyrus, CST extending into the pre/postcentral gyrus, superior

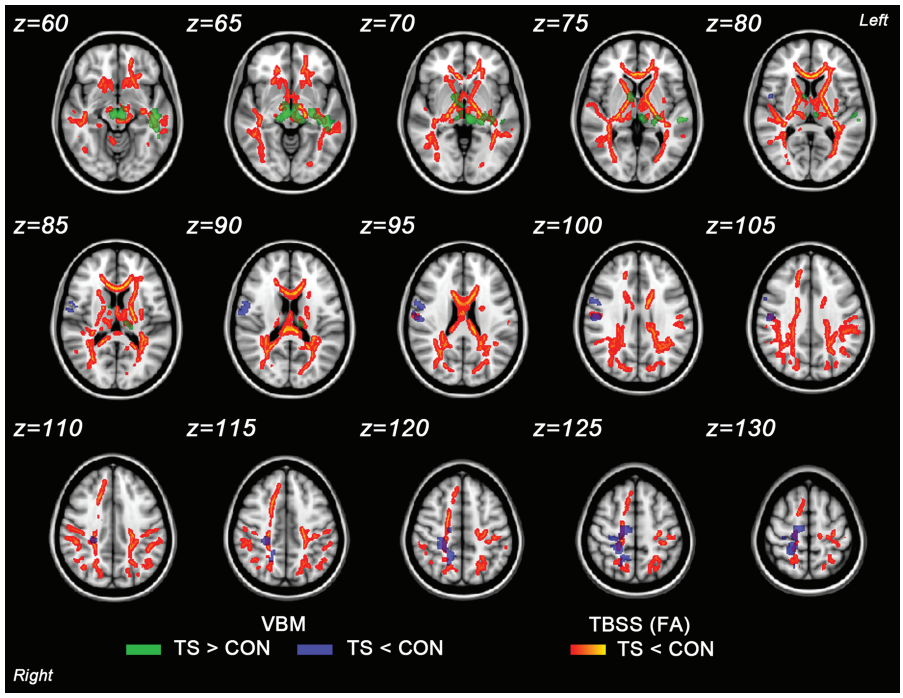

Figure 1. Superimposed results of voxels showing significant FA reduction in TBSS and VBM clusters showing significant WMV differences between the groups (P < 0.05, FWE corrected). Group differences in TBSS were "thickened" (for visualization purposes) by expanding the significant WM skeleton cluster to the full extent of the local FA map. 1) FA reduction in TS relative to controls (CON) is shown in red–yellow. 2) Greater WMV in TS relative to CON is shown in green. 3) Reduced WMV in TS relative to CON is shown in blue. Results are mapped onto a standard T_1 Montreal Neurological Institute 152 template.

parietal lobule WM and precuneus WM. In contrast, significant enlargement in WMV ($P < 0.05$, FWE corrected) in TS relative to controls was observed bilaterally in the anterior thalamic radiation and unilaterally in the left SLF, ILF, IFO, sagittal stratum, posterior limb of the internal capsule, fusiform WM, and superior/middle/inferior temporal gyrus WM and the right ALIC (Fig. 1).

Behavioral Correlations

Within the TS group, there was a significant positive correlation between FA in the left SLF ROI (derived from the atlas-based analysis) and the WISC-IV/WPPSI-III Block Design scores (standardized $\beta = 0.526$, $P = 0.033$). There was also a significant positive correlation between FA in the left ALIC ROI and the Wide Range Assessment of Visual Motor Abilities (Adams 1995) Pegboard score (standardized $\beta = 0.49$, $P = 0.02$). There were no significant associations between AD/RD values and cognitive measures.

Discussion

In this study, we used 2 image acquisition techniques and complementary image analysis methods to investigate WM structure in prepubertal, nonmosaic, estrogen-naive girls with TS compared with controls. TS had extensive overlap between regions of WM structure aberrations (obtained from DTI) and regions of WMV aberrations (obtained from anatomical MRI) (Fig. 2). Specifically, TBSS, VBM, and post hoc atlas-based analyses consistently showed WM aberrations in the SLF and fusiform. Overlapping regions between TBSS and VBM were seen in the ILF, IFO, IC, and CST. TBSS and post hoc atlas-based analyses both demonstrated aberrant WM structure in the CC, tapetum, ALIC, and STG. These overlapping brain regions may be associated with difficulties in visual, sensorimotor, and social functions in girls with TS. This premise is supported by the statistical association of visuospatial performance with WM integrity of the SLF and fine motor abilities with WM integrity of the IC in our TS group.

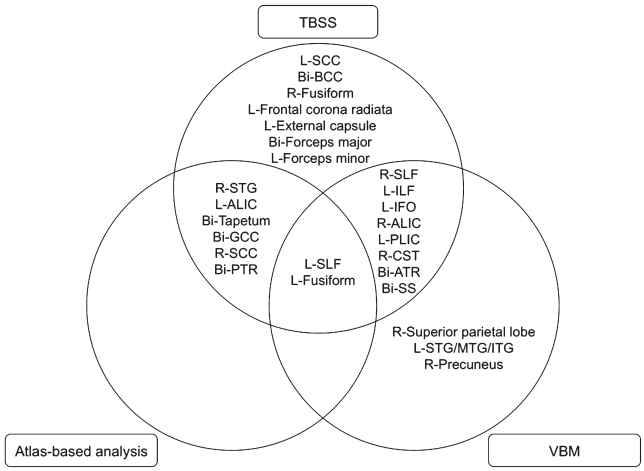

Figure 2. Diagram showing nature of overlapping results from multiple analytical techniques investigating WM structure and volume in TS. Bi, bilateral; L, left; R, right; SCC, splenium of corpus callosum; BCC, body of corpus callosum; GCC, gene of corpus callosum; SLF, superior longitudinal fasciculus; ILF, inferior longitudinal fasciculus; IFO, inferior fronto-occipital fasciculus; ALIC, anterior limb of the internal capsule; PLIC, posterior limb of the internal capsule; CST, corticospinal tract; ATR, anterior thalamic radiation; PTR, posterior thalamic radiation; SS, sagittal stratum; STG, superior temporal gyrus; MTG, middle temporal gyrus; ITG, inferior temporal gyrus.

Visuospatial difficulties are commonly observed in females with TS (Kesler 2007). In this study, all analysis methods consistently showed WM aberrations in TS in the left SLF in a location consistent with that of SLFII, which is part of the dorsal visual stream. This pathway is important for visuospatial processing, attention, and awareness (Schmahmann and Pandya 2006). The SLF is composed of 4 subpathways: the SLF I, II, and III, and the arcuate fasciculus. The differences detected in this study appear to be located primarily in SLF II and/or SLF III (Makris et al. 2005). In our TS sample, there also was a positive correlation between FA values of the left SLF and the WISC/WPPSI Block Design score. Our findings are consistent with the previous findings of decreased FA in the left SLF in adolescent and young adults with TS receiving estrogen therapy (Holzapfel et al. 2006). This converging evidence suggests that the SLF fiber bundle is affected in TS throughout childhood and adolescence, pre- and post-estrogen therapy, and that visuospatial abilities among girls with TS are associated with abnormal WM structure along the SLF. This finding is also consistent with previous studies reporting unchanged visuospatial skills following estrogen treatment in girls with TS (Ross et al. 1998).

An additional aberrant WM pathway in TS potentially important for visual abilities includes the splenium of the CC and tapetum (TBSS and atlas-based analysis). The splenium of the CC connects the posterior parietal and the occipital lobes and is crucial for the interhemispheric transfer of visual information (Fabri et al. 2011), whereas the tapetum is a thin rim of bidirectional CC fibers connecting the temporal and occipital lobes (Schmahmann and Pandya 2006) and transfers visual information from the visual cortex to the contralateral temporal lobe (Tusa and Ungerleider 1985). Our results suggest that impairments in interhemispheric transfer, as well as local processing of visual information, contribute to the visual difficulties in TS.

The ILF is another pathway involved in visual function that was significantly different between groups in the TBSS and VBM analyses. The ILF is associated with the occipitotemporal visual stream and is related to object and face recognition and discrimination (Schmahmann and Pandya 2006). Thus, our finding of the left ILF may also be associated with difficulties in face recognition reported in TS (Rae et al. 2004). Important components of face recognition are also attributed to the fusiform gyrus (Kanwisher et al. 1997). Impaired face recognition in TS may be associated with our results of aberrant WM structure and WMV in the left fusiform from TBSS, VBM, and post hoc atlas-based analyses. Specifically, for TS, a previous fMRI study of fearful face processing demonstrated that impaired appraisal of facial affect and habituation to fearful stimuli may stem from impaired functional connectivity between the left fusiform gyrus and left medial amygdala (Skuse et al. 2005). In our study, TBSS showed aberrant WM structure between the fusiform and amygdala in TS, which suggests that aberrant connectivity between these 2 regions may contribute to impairment in fearful face processing. Taken together, our current findings provide additional evidence suggesting aberrant WM connectivity in pathways important for visuospatial abilities and face processing in TS.

Sensorimotor function is also known to be impaired in TS. Specifically, females with TS have difficulties in gross and fine motor function, joint stability, gait, and muscle strength

(Nijhuis-van der Sanden et al. 2003). In our study, girls with TS had abnormal WM structure in the left ALIC demonstrated by TBSS and post hoc atlas-based analyses. In addition, there was a significant positive correlation between the degree of the left ALIC anomalies and the level of fine motor deficits in TS. The present results of decreased FA values in the IC were consistent with our previous finding from girls, adolescents, and young adults with TS (Holzapfel et al. 2006). In addition, we observed new findings of aberrant WM structure and WMV of the CST in TS, which contains sensorimotor pathways. These findings suggest that aberrations of WM structure and connectivity in the sensorimotor pathway may contribute to motor problems in TS.

Impairments in social functioning have been consistently noted among females with TS (McCauley et al. 2001). Social difficulties in girls with TS may partially stem from problems with face and emotion processing as well as with the interpretation of gaze and empathy (Lawrence, Campbell, et al. 2003; Lawrence, Kuntsi, et al. 2003). These impairments may in turn be a result of abnormal brain structure in regions important for visual and face processing as described above as well as in regions involved in social cognition. For instance, the STG, which showed significant between-group differences in TBSS and post hoc atlas-based analysis, is involved in information processing related to the changeable configurations of faces (Adolphs 2003). The STG also has substantial connections with the amygdala, and both are strongly implicated in social perception and theory of mind (Allison et al. 2000; Adolphs 2009). Taken together, our current results suggest that WM aberrations in the STG, together with aberrant visual and face processing abilities, may be associated with impaired emotion recognition in girls with TS.

In this study, we attempted to overcome some of the limitations of single analytical approaches by using 4 different image-processing techniques with 2 different imaging modalities (DTI and anatomical MRI). Each analytical approach has advantages and disadvantages. Thus, a thorough investigation using different approaches potentially provides complementary information that can more accurately depict how WM is affected in TS. The atlas-based analysis has the advantage of having better statistical power compared with multiple voxel-wise comparisons because it reduces the location information from hundreds of thousands of voxels to a limited number of ROIs. Furthermore, in contrast to whole brain voxel-wise analyses, the atlas-based analysis averages voxel values within each WM region segmented by the atlas and is more likely to detect differences that are spread throughout segmented WM regions, except where these differences straddle a boundary between 2 segments, each of which they only partial fill. On the other hand, when changes in DTI diffusivities are confined to a very small area or do not follow the anatomical boundaries segmented by the atlas, TBSS has the advantage of being able to detect fine changes in WM more clearly because it is a voxel-wise analysis. These fundamental differences in methodology are a likely reason for discrepancy in the results between TBSS and atlas-based analysis. In addition, using TBSS, we observed that increased RD largely overlapped with reduced FA in the TS group. Furthermore, WM regions showing increased AD did not overlap with those of FA/RD changes. Although these findings suggest that WM aberrations in TS may arise primarily from changes in fiber integrity and myelination and not changes in fiber coherence (Song et al. 2002), it is not possible to determine the precise underlying histological structure of WM based solely on this imaging technique. Changes in FA are related to a combination of factors such as changes in fiber diameter, density, myelination, coherence, and extracellular diffusion. Therefore, simultaneous DTI and VBM analyses raise important hypotheses and implications for understanding WM histology in TS. Increased WMV with reduced FA is likely to be influenced by glial proliferation, increased axonal diameter, and fiber crossing, whereas decreased WMV with reduced FA may be associated with reduced myelination and decreased axon density (Schmierer et al. 2007; Sierra et al. 2011). These neuroimaging findings suggest that WM microstructural aberrations in TS may have different underlying histology in different brain regions; however, additional studies, using direct visualization of postmortem brain tissue, are needed to determine the specific histology of WM in TS.

In contrast to the findings presented here, some previous studies have reported functional and structural abnormalities in brain regions related to executive and memory functions (Murphy et al. 1993; Kesler, Haberecht, et al. 2004; Hart et al. 2006). These discrepant findings may result from variation in participant characteristics, neuroimaging acquisition techniques, and neuroimaging analysis methods. For example, these prior studies used pubertal or adult participants with TS including mosaic and nonmosaic genotypes. In addition, they included women with TS receiving estrogen therapy at the time of the study. In contrast, our study included only prepubertal, estrogen-naive, and nonmosaic TS participants to avoid the confound of exogenous estrogen therapy on brain maturation as well as on cognitive and motor functions (Toran-Allerand 1991; Ross et al. 1998). Furthermore, mosaic karyotypes can contribute to a "X chromosome dosage effect" and cause broad heterogeneity in physical and cognitive manifestations of TS (Murphy et al. 1997; Kesler et al. 2003). However, variation in the length and dosages of GH therapy is still a confounding factor. The influence of GH therapy on WM development and cognitive function in TS has not yet been reported; however, Cutter et al. (2006) suggested that GH therapy increases regional GMV in TS. Therefore, future studies should address the effect of the variation in GH therapy to avoid confounding effects. Moreover, because of sample size, we did not investigate the effect of X-linked imprinting on WM development in girls with TS. Thus, further research is warranted regarding how parental origin of the X chromosome plays a role in WM development in girls with TS.

In summary, our findings indicate that complete absence of an X chromosome in young females (prior to receiving exogenous estrogen) is associated with WM aberrations in specific regions implicated in the characteristic cognitive phenotypes of TS. In addition, previous postmortem studies indicate that typically developing girls have increased ovarian estrogen concentration in the first year of life, analogous to the testosterone surge in the first 6 months of life in boys (Bidlingmaier et al. 1987); however, girls with TS lack this surge. This estrogen deficiency from a very early age could also influence aberrant WM development in TS. Therefore, future studies with larger sample, wide-age rage, and longitudinal design are required to elucidate how estrogen therapy would modify WM aberration in TS. Current research offers insight into the X-linked genetic and hormonal influences on cognitive, behavioral, and brain development not only in TS but also in male-based sex chromosome aneuploidy disorders (e.g., 47, XXY; Klinefelter syndrome). Finally, our findings may

improve our understanding of the neuroanatomical basis underlying deficits in visual, sensorimotor, and social functions in TS.

Funding

National Institute of Health (5-R01-HD049653 to A.L.R); Chain of Love Foundation (to A.L.R); American Psychiatric Institute for Research and Education/Lilly Psychiatric Research Fellowship Award (to D.S.H.); National Institute of Mental Health (T32–MH19908 to A.L.R., D.S.H).

Notes

The authors thank Bria Dunkin and Kristen Sheau for their contributions in data collection. *Conflict of Interest*: None declared.

References

Adams W. 1995. Wide range assessment of visual motor abilities. Wilmington (DE): Wide Range Inc.

Adolphs R. 2003. Cognitive neuroscience of human social behaviour. Nat Rev Neurosci. 4:165–178.

Adolphs R. 2009. The social brain: neural basis of social knowledge. Annu Rev Psychol. 60:693–716.

Allison T, Puce A, McCarthy G. 2000. Social perception from visual cues: role of the STS region. Trends Cogn Sci. 4:267–278.

Ashburner J. 2007. A fast diffeomorphic image registration algorithm. Neuroimage. 38:95–113.

Ashburner J, Friston KJ. 2005. Unified segmentation. Neuroimage. 26:839–851.

Basser PJ, Mattiello J, LeBihan D. 1994. MR diffusion tensor spectroscopy and imaging. Biophys J. 66:259–267.

Bidlingmaier F, Strom TM, Dorr HG, Eisenmenger W, Knorr D. 1987. Estrone and estradiol concentrations in human ovaries, testes, and adrenals during the first two years of life. J Clin Endocrinol Metab. 65:862–867.

Ceritoglu C, Oishi K, Li X, Chou MC, Younes L, Albert M, Lyketsos C, van Zijl PC, Miller MI, Mori S. 2009. Multi-contrast large deformation diffeomorphic metric mapping for diffusion tensor imaging. Neuroimage. 47:618–627.

Constantino JN, Davis SA, Todd RD, Schindler MK, Gross MM, Brophy SL, Metzger LM, Shoushtari CS, Splinter R, Reich W. 2003. Validation of a brief quantitative measure of autistic traits: comparison of the social responsiveness scale with the autism diagnostic interview-revised. J Autism Dev Disord. 33:427–433.

Cutter WJ, Daly EM, Robertson DM, Chitnis XA, van Amelsvoort TA, Simmons A, Ng VW, Williams BS, Shaw P, Conway GS, et al. 2006. Influence of X chromosome and hormones on human brain development: a magnetic resonance imaging and proton magnetic resonance spectroscopy study of Turner syndrome. Biol Psychiatry. 59:273–283.

Fabri M, Polonara G, Mascioli G, Salvolini U, Manzoni T. 2011. Topographical organization of human corpus callosum: an fMRI mapping study. Brain Res. 1370:99–111.

Faria AV, Zhang J, Oishi K, Li X, Jiang H, Akhter K, Hermoye L, Lee SK, Hoon A, Stashinko E, et al. 2010. Atlas-based analysis of neurodevelopment from infancy to adulthood using diffusion tensor imaging and applications for automated abnormality detection. Neuroimage. 52:415–428.

Gravholt CH. 2005. Clinical practice in Turner syndrome. Nat Clin Pract Endocrinol Metab. 1:41–52.

Haberecht MF, Menon V, Warsofsky IS, White CD, Dyer-Friedman J, Glover GH, Neely EK, Reiss AL. 2001. Functional neuroanatomy of visuo-spatial working memory in Turner syndrome. Hum Brain Mapp. 14:96–107.

Hart SJ, Davenport ML, Hooper SR, Belger A. 2006. Visuospatial executive function in Turner syndrome: functional MRI and neurocognitive findings. Brain. 129:1125–1136.

Hayasaka S, Phan KL, Liberzon I, Worsley KJ, Nichols TE. 2004. Nonstationary cluster-size inference with random field and permutation methods. Neuroimage. 22:676–687.

Holzapfel M, Barnea-Goraly N, Eckert MA, Kesler SR, Reiss AL. 2006. Selective alterations of white matter associated with visuospatial and sensorimotor dysfunction in turner syndrome. J Neurosci. 26:7007–7013.

Jiang H, van Zijl PC, Kim J, Pearlson GD, Mori S. 2006. DtiStudio: resource program for diffusion tensor computation and fiber bundle tracking. Comput Methods Programs Biomed. 81:106–116.

Kanwisher N, McDermott J, Chun MM. 1997. The fusiform face area: a module in human extrastriate cortex specialized for face perception. J Neurosci. 17:4302–4311.

Kesler SR. 2007. Turner syndrome. Child Adolesc Psychiatr Clin N Am. 16:709–722.

Kesler SR, Blasey CM, Brown WE, Yankowitz J, Zeng SM, Bender BG, Reiss AL. 2003. Effects of X-monosomy and X-linked imprinting on superior temporal gyrus morphology in Turner syndrome. Biol Psychiatry. 54:636–646.

Kesler SR, Garrett A, Bender B, Yankowitz J, Zeng SM, Reiss AL. 2004. Amygdala and hippocampal volumes in Turner syndrome: a high-resolution MRI study of X-monosomy. Neuropsychologia. 42:1971–1978.

Kesler SR, Haberecht MF, Menon V, Warsofsky IS, Dyer-Friedman J, Neely EK, Reiss AL. 2004. Functional neuroanatomy of spatial orientation processing in Turner syndrome. Cereb Cortex. 14:174–180.

Korkman M, Kirk U. 1998. NEPSY: a developmental neuropsychological assessment. San Antonio (TX): The Psychological Corporation.

Korkman M, Kirk U. 2007. NEPSY-second edition (NEPSY-II). San Antonio (TX): The Psychological Corporation.

Lawrence K, Campbell R, Swettenham J, Terstegge J, Akers R, Coleman M, Skuse D. 2003. Interpreting gaze in Turner syndrome: impaired sensitivity to intention and emotion, but preservation of social cueing. Neuropsychologia. 41:894–905.

Lawrence K, Kuntsi J, Coleman M, Campbell R, Skuse D. 2003. Face and emotion recognition deficits in Turner syndrome: a possible role for X-linked genes in amygdala development. Neuropsychology. 17:39–49.

Makris N, Kennedy DN, McInerney S, Sorensen AG, Wang R, Caviness VS, Pandya DN. 2005. Segmentation of subcomponents within the superior longitudinal fascicle in humans: a quantitative, in vivo, DT-MRI study. Cereb Cortex. 15:854–869.

McCauley E, Feuillan P, Kushner H, Ross JL. 2001. Psychosocial development in adolescents with Turner syndrome. J Dev Behav Pediatr. 22:360–365.

Molko N, Cachia A, Riviere D, Mangin JF, Bruandet M, LeBihan D, Cohen L, Dehaene S. 2004. Brain anatomy in Turner syndrome: evidence for impaired social and spatial-numerical networks. Cereb Cortex. 14:840–850.

Mori S, Crain BJ, Chacko VP. 1999. Three-dimensional tracking of axonal projections in the brain by magnetic resonance imaging. Ann Neurol. 45:265–269.

Murphy DG, DeCarli C, Daly E, Haxby JV, Allen G, White BJ, McIntosh AR, Powell CM, Horwitz B, Rapoport SI. 1993. X-chromosome effects on female brain: a magnetic resonance imaging study of Turner's syndrome. Lancet. 342:1197–1200.

Murphy DG, Mentis MJ, Pietrini P, Grady C, Daly E, Haxby JV, De La Granja M, Allen G, Largay K, White BJ, et al. 1997. A PET study of Turner's syndrome: effects of sex steroids and the X chromosome on brain. Biol Psychiatry. 41:285–298.

Nichols TE, Holmes AP. 2002. Nonparametric permutation tests for functional neuroimaging: a primer with examples. Hum Brain Mapp. 15:1–25.

Nijhuis-van der Sanden MW, Eling PA, Otten BJ. 2003. A review of neuropsychological and motor studies in Turner Syndrome. Neurosci Biobehav Rev. 27:329–338.

Oishi K, Faria A, Jiang H, Li X, Akhter K, Zhang J, Hsu JT, Miller MI, van Zijl PC, Albert M, et al. 2009. Atlas-based whole brain white matter analysis using large deformation diffeomorphic metric mapping: application to normal elderly and Alzheimer's disease participants. Neuroimage. 46:486–499.

Rae C, Joy P, Harasty J, Kemp A, Kuan S, Christodoulou J, Cowell CT, Coltheart M. 2004. Enlarged temporal lobes in Turner syndrome: an X-chromosome effect? Cereb Cortex. 14:156–164.
Raznahan A, Cutter W, Lalonde F, Robertson D, Daly E, Conway GS, Skuse DH, Ross J, Lerch JP, Giedd JN, et al. 2010. Cortical anatomy in human X monosomy. Neuroimage. 49:2915–2923.
Reynolds CR, Richmond BO. 1997. What I think and feel: a revised measure of children's manifest anxiety. J Abnorm Child Psychol. 25:15–20.
Ross JL, Roeltgen D, Feuillan P. 1998. Effects of estrogen on nonverbal processing speed and motor function in girls with Turner's syndrome. J Clin Endocrinol Metab. 83:3198–3204.
Schmahmann J, Pandya D. 2006. Fiber pathways of the brain. New York (NY): Oxford University Press.
Schmierer K, Wheeler-Kingshott CA, Boulby PA, Scaravilli F, Altmann DR, Barker GJ, Tofts PS, Miller DH. 2007. Diffusion tensor imaging of post mortem multiple sclerosis brain. Neuroimage. 35:467–477.
Sierra A, Laitinen T, Lehtimki K, Rieppo L, Pitkanen A, Grohn O. 2011. Diffusion tensor MRI with tract-based spatial statistics and histology reveals undiscovered lesioned areas in kainate model of epilepsy in rat. Brain Struct Funct. 216:123–135.
Skuse DH, James RS, Bishop DV, Coppin B, Dalton P, Aamodt-Leeper G, Bacarese-Hamilton M, Creswell C, McGurk R, Jacobs PA. 1997. Evidence from Turner's syndrome of an imprinted X-linked locus affecting cognitive function. Nature. 387:705–708.
Skuse DH, Morris JS, Dolan RJ. 2005. Functional dissociation of amygdala-modulated arousal and cognitive appraisal, in Turner syndrome. Brain. 128:2084–2096.
Smith SM, Jenkinson M, Johansen-Berg H, Rueckert D, Nichols TE, Mackay CE, Watkins KE, Ciccarelli O, Cader MZ, Matthews PM, et al. 2006. Tract-based spatial statistics: voxelwise analysis of multi-subject diffusion data. Neuroimage. 31:1487–1505.
Smith SM, Nichols TE. 2009. Threshold-free cluster enhancement: addressing problems of smoothing, threshold dependence and localisation in cluster inference. Neuroimage. 44:83–98.
Song SK, Sun SW, Ramsbottom MJ, Chang C, Russell J, Cross AH. 2002. Dysmyelination revealed through MRI as increased radial (but unchanged axial) diffusion of water. Neuroimage. 17:1429–1436.
Talairach J, Tournoux P. 1988. Co-planar stereotaxic atlas of the human brain: 3-dimensional proportional system: an approach to cerebral imaging. New York: Thieme Medical Publishers.
Toran-Allerand CD. 1991. Organotypic culture of the developing cerebral cortex and hypothalamus: relevance to sexual differentiation. Psychoneuroendocrinology. 16:7–24.
Tusa RJ, Ungerleider LG. 1985. The inferior longitudinal fasciculus: a reexamination in humans and monkeys. Ann Neurol. 18:583–591.
Wakana S, Jiang H, Nagae-Poetscher LM, van Zijl PC, Mori S. 2004. Fiber tract-based atlas of human white matter anatomy. Radiology. 230:77–87.
Wechsler D. 2002. Wechsler Preschool and Primary Scale of Intelligence-Third Edition (WPPSI-III). San Antonio (Tx): The Psychological Corporation.
Wechsler D. 2003. Wechsler Intelligence Scale for Children-Fourth Edition (WISC-IV). San Antonio (Tx): The Psychological Corporation.
Woods RP, Grafton ST, Holmes CJ, Cherry SR, Mazziotta JC. 1998. Automated image registration: I. General methods and intrasubject, intramodality validation. J Comput Assist Tomogr. 22:139–152.
Zhang Y, Brady M, Smith S. 2001. Segmentation of brain MR images through a hidden Markov random field model and the expectation-maximization algorithm. IEEE Trans Med Imaging. 20:45–57.